# Analysis and testing of tread braked railway wheel — Effects of hot spots on wheel performance

(article starts on next page)

# Analysis and testing of tread braked railway wheel — Effects of hot spots on wheel performance

Eric Voortman Landström [*], Tore Vernersson, Roger Lundén

*CHARMEC/Department of Mechanics and Maritime Sciences, Chalmers University of Technology, Gothenburg, SE-41296, Sweden*

## ARTICLE INFO

## ABSTRACT

To investigate the impact of localised heating phenomena in the form of hot spots on wheel performance in general and on wheel residual stress state in particular, a combination of experimental testing and finite element simulations of tread braked wheels has been performed. Using a newly established full-scale railway brake test rig, a wheel is exposed to prolonged drag braking applications at constant power levels to induce high temperatures on the wheel tread. The distribution and evolution of the temperature is studied using a high-speed, high-resolution thermographic camera in addition to traditional sliding thermocouples. Measured temperature data are then used in combination with a thermomechanically calibrated material model to simulate the wheel behaviour. For this purpose, a 3D finite element model representing a sector of a railway wheel is used. The experimental results show that the temperatures measured utilising sliding thermocouples provide insufficient information since they cannot resolve the uneven tread temperatures given typical response times. Non-uniform heating is found to have a significant effect on tensile residual stresses in the rim. Especially the case with global uneven temperatures is found to generate potentially hazardous residual stresses. The results presents future challenges for the analysis and development of the brake-wheel-rail system.

## 1. Introduction

Tread brakes provide a low-cost and maintenance efficient braking system and are commonly used in both freight and passenger railway vehicles. However, elevated wheel temperatures occur during drag braking actions due to the frictional heating [1,2]. Such prolonged braking, whether due to system malfunctions or flawed driver behaviour, could possibly result in situations where the mechanical strength of the wheel is jeopardised by elevated temperatures. Specifically, material plastificiation due to restricted thermal expansion in combination with material deterioration occurring at high temperature levels, can create significant tensile residual stresses. The circumferential stresses in the wheel rim are compressive from manufacturing and become increasingly so during braking as the wheel rim temperature increases. Plastificiation may then occur in compression, creating conceivably dangerous levels of tensile residual stresses when the wheel cools down. This residual stress field is highly dependent on the thermal power flowing into the wheel tread during prolonged braking. The European norm for approval of forged railway wheels states that +275 MPa (average in rim) is the highest allowable tensile residual stress for a worn wheel [3].

The thermomechanical interaction between friction materials and rotors has been extensively studied over the years for both block brakes and disc brakes [1,2,4–12]. Due to the difficulties in modelling of the frictional contact behaviour and its thermal effects, most models for predicting the temperature evolution account for heating in an average sense. The thermal power is therefore modelled as evenly distributed over the contact surface of friction materials and rotors using a presumed (constant) contact pressure and coefficient of friction. Nonetheless, it is well known that the contact pressure is not even and that hot spots and other types of frictionally induced ThermoElastic Instabilities (TEI), with significantly elevated local temperatures, are formed during braking [8,9,12–15].

Thermoelastic instabilities arise when a small area is subjected to somewhat higher contact pressure than its surrounding area, thus being heated to a higher temperature. The small region will then protrude due to thermal expansion, further concentrating the contact pressure. High wear and/or low friction heat slows or stops the process. The wavelength of the hot spots in the circumferential direction is often corresponding to approximately a half-length of a composite (sintered or organic) brake block [10], but the thermoelastic interaction can also produce different forms of temperature patterns on the tread such as bands [12]. There are also results showing that other forms of nonuniformities can occur, e.g. leading to significant temperature differences over larger sections of the wheel [16].
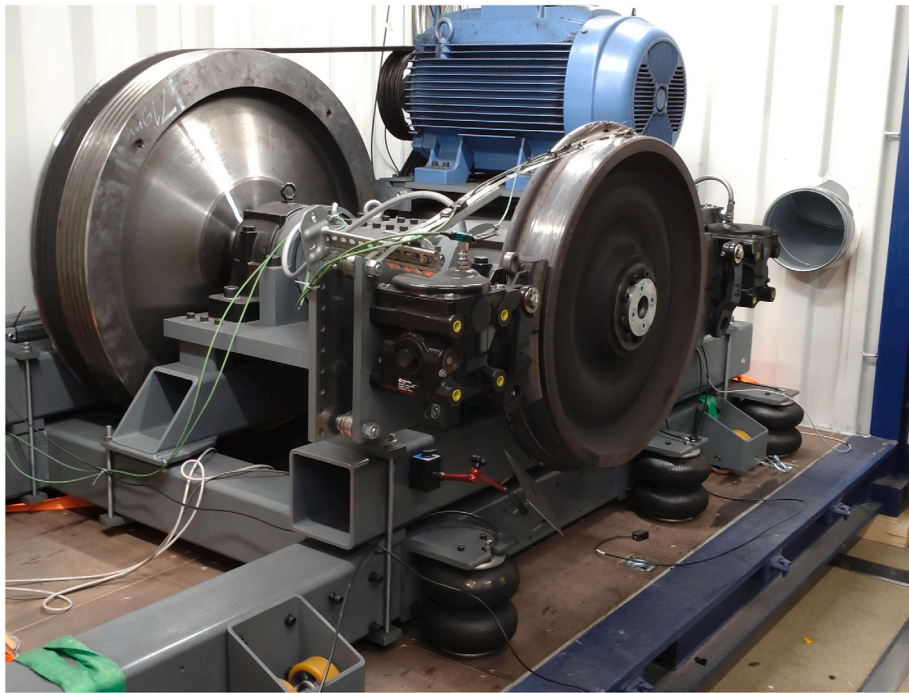
---

**Fig. 1.** Brake test rig at Chalmers.

Issues arise at modelling since the contact pressure is not uniform, with only a small part of the brake block being in effective contact with the wheel. As mentioned, this tends to be ignored in modelling as it is simpler to use uniform contact conditions. Generally disregarded is also the effect that the brake block frictional heat produces a fast moving heat source on the wheel tread. Investigations have shown [10] that this effect has a minor effect on wheel–rail–block heat partitioning, but that it has a massive impact on computational efficiency. For this reason, models actually simulating moving heat sources on the tread are generally avoided and instead models that account for rotational effects from heat sources in an average sense are favoured, often using axisymmetric representation of the wheel. Thus, the effect these hot spots has on the subsequent residual stress field in railway wheels is not well investigated due to the difficulties in both experimentally measuring and numerically modelling the contact and the related temperature field. Furthermore, accurate models of the wheel steel and the friction material and their interaction are needed for the study of these phenomena. The increased temperatures and residual stresses constitute potential risks for thermally aggravated RCF and tentatively also for global wheel fracture [13,17].

In the current paper a combined experimental–numerical research effort is launched to investigate wheel performance for observed thermoelastic instabilities for brake rig conditions, thus ignoring wheel–rail contact effects. A combination of a high-resolution, high frame rate thermographic camera [18] and sliding thermocouples on the wheel tread is used to capture the temperature variation on both the wheel tread and the field side of the wheel rim. Circumferential residual stresses in the wheel rim are measured using the elastoacoustic effect [19].

The experimental results are used as a basis for a modelled heat flux distribution on the tread of a thermal 3D finite element (FE) model of a wheel segment. The almost stationary hot spot patterns on the wheels, often observed in the experiments, are exploited. This allows for straightforward analysis without overly increasing computational complexity. The effects of varying size and intensity of hot spots are studied, in order to better draw conclusions from the experiments.

The temperature results from the thermal FE model is finally employed in a sequentially coupled thermomechanical FE analysis. The

FE model is employing a viscoplastic Chaboche [20,21] material model that has been calibrated using both isothermal and anisothermal thermomechanical experiments performed on ER7 wheel steel specimens [22].

The present paper is organised as follows: In Chapter 2 the experimental method is introduced, with focus on temperature measurements on a tread braked wheel. In Chapter 3 the thermal and mechanical finite element models are described. In Chapter 4 the experimental results are presented together with results from the FE simulations employing the thermal and the mechanical FE models. In chapter 5 the results are discussed and in Chapter 6 conclusions are given.

## 2. Experimental testing

The testing is performed using a novel brake test rig designed within our research centre CHARMEC and assembled at Chalmers University of Technology. The power is provided by a 105 kW electric motor coupled to the wheel axle by a belt drive. This gives a velocity of 60 km/h at the wheel tread when the motor is running at nominal speed 1500 rpm. Two SAB WABCO BFC tread brake units (4th generation) are mounted on free-swinging arm supported by ball bearings. The arm is constrained from rotation by a force transducer providing the braking torque. The possible brake force ranges from 0 kN at 0–0.25 bar to 50 kN at 5 bar braking pneumatic pressure. The setup is shown in Fig. 1, with the brake blocks mounted in a 2xBg configuration (a single brake block on each side of the wheel). Organic composite [23] brake blocks are used, of a type having high wear resistance at higher temperatures [24]. Note that this block does not fulfil the requirements for composite blocks as stipulated in UIC Leaflet 541-4 [25] since it does not fulfil requirements on acting as a thermal fuse to protect the wheel. However, they are widely used for these kinds of tests and proposed in the latest (draft) version of EN 13979-1 [24]. The block's nominal frictional coefficient between the wheel and the block varies between 0.25 and 0.3 depending on e.g. speed and temperature [23]. The tests are performed at average brake power levels 30 kW and 50 kW and at a constant speed 60 km/h of the wheel running surface. The speed and higher power level are as defined in EN 13979-1 [3], whereas the lower power level is chosen to give temperatures more
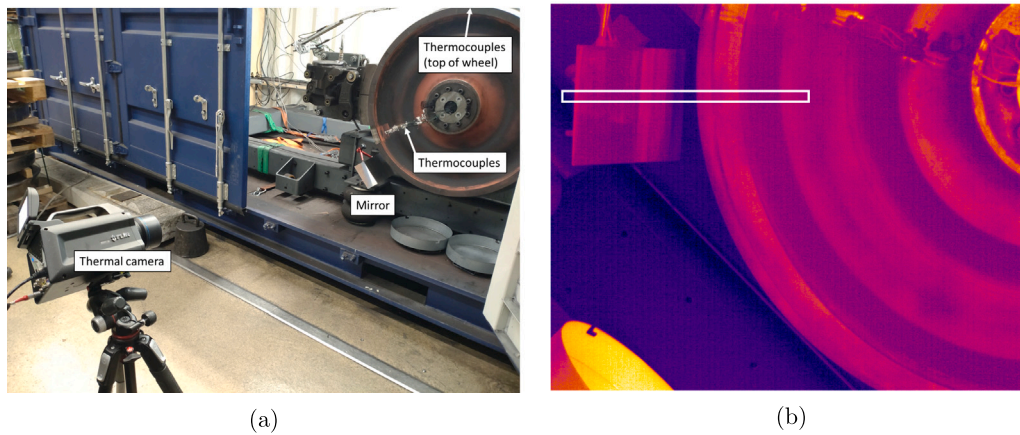
**Fig. 2.** Figure showing the camera setup, (a) the camera relative to the wheel, (b) the slit in the protective container through which the wheel radius and mirror is seen and (c) the full view of the camera when the door is open. The white rectangle indicates the approximate pixels that are captured during measurements.

related to standard revenue service. Data acquisition is performed by a National Instruments Compact DAQ device [26] and the brake power is controlled using a measurement programme written in LabView [27].

The temperatures are measured using two separate and complementary methods. Two sliding thermocouples are put into contact with the rotating wheel tread, giving emissivity-independent measurements of tread temperatures. Because of the large time constant of the thermocouples, it is not possible to resolve rapid changes in the temperature distribution. A FLIR X8400sc thermographic camera [18] is simultaneously used to measure wheel rim (field side) and tread temperature (via a stainless steel sheet metal mirror) distributions. For the tread an estimated surface radiation emissivity is employed, which was calibrated by comparing average radiometric tread temperatures to those given by two sliding thermocouples. The steel mirror is a reasonable IR reflector with a reflectance of roughly 0.9 [28] and the errors are thus relatively low after calibration. The mirror also requires periodic dusting to preserve the reflectance.

The camera is set into a so-called sub-window scanning mode of $8 \times 1280$ pixels and a frame rate of 2000 Hz, scanning a radial line on the wheel and the mirror. Given the rotational velocity of the tested wheel of 60 km/h, this gives a spatial resolution per frame of roughly 8 mm in the circumferential direction. This is sufficient for resolving the highly varying temperature distribution on the wheel tread and for detecting any hot spots. Additionally, for one 30 kW test, the camera is set to capture one image of the entire field side of the wheel approximately every 30 revolutions at the full resolution of $1280 \times 1024$ pixels, then employing a $60 \times 15$ cm mirror below the wheel to show a larger part of the tread. See Fig. 2 for the approximate positioning of the camera with regards to the dynamometer.

Four test runs are performed on a freight wheel, made from ER7, wheel steel machined to diameter 840 mm (limit diameter in operation, new diameter 920 mm) where the three first runs have braking power 30 kW for 45 min and the fourth run 50 kW for 40 min. Since the wheel was mounted also during initial tests of the newly established brake rig, the wheel had been subjected to somewhat elevated temperatures prior to tests reported here. This is reflected in the measured residual stresses in the wheel rim before the first test run, showing a tensile stress state rather than a compressive one, that would be found in a virgin wheel machined to the limit diameter. The wheel is coated using a high-temperature resistant spray-paint in order to attain a well-defined emissivity everywhere but the tread. In this study, an emissivity 1.0 is employed for all surfaces during measurement, and is then corrected by post-processing, exploiting thermocouple data collected during cooling.

The data from the thermocamera are synchronised with the wheel angular position using (1) an unpainted area on field side of the wheel rim (circumferential length 8 cm), which can readily be identified in

thermographs owing to its lower emissivity (i.e., with a lower apparent temperature), or (2) a once-per-revolution electric pulse that triggers saving of data. The synchronisation method employed depends on camera sampling mode.

The circumferential residual stresses are measured using an ultrasonic device [19]. It uses the elasto-acoustic method which is the standard NDT-method for determining the residual circumferential stresses in tread braked wheels. It assesses the average stress over the entire width of the wheel rim, from rim front face to flange back. Two measurements are taken every 2 cm over two 50 cm long lines at different depths below the running surface on the field side of the wheel rim. The stress state is almost uniaxial as the radial and axial stresses are substantially lower than the circumferential ones.

## 3. Modelling

The modelling is performed using the commercial FE software ABAQUS [29]. The heat flux is applied to the tread surface defined via the ABAQUS Fortran subroutine DFLUX to mimic observed temperature variations. The heat flux input is defined as

$$q = q_{bg} + q_{hs} \left[ 1 - \left( \frac{x}{a} \right)^2 - \left( \frac{y}{b} \right)^2 \right]^{\frac{1}{2}} \qquad (1)$$

where $q_{bg}$ is the background heat over the wheel tread, the $q_{hs}$–term is for the heat flux superimposed at the hot spot. Thus, the heat flux is defined over an ellipse at the centre of the tread of a 20° segment of the wheel, see Fig. 3, where $a$ and $b$ are the circumferential and axial semiaxes respectively. The sector angle corresponds to a hot spot wavelength of roughly 14.7 cm. The obtained heat distribution allows for simulation of observed hot spot temperatures at testing. Further, minimum tread temperatures correspond to the background heat flux $q_{bg}$ away from hot spots. The total heat to the wheel segment is kept constant by reducing $q_{bg}$, based on $q_{hs}$ and hot spot size.

The temperature results are then used as prescribed conditions in the so-called sequentially-coupled thermal–mechanical analyses. The sequential analysis is used as both traction (3000 N at 50 kW, 60 km/h giving 0.06 MPa traction stress) and brake force (6000 kN per side giving average 0.23 normal stress) are negligible in comparison to compressive circumferential stresses from thermomechanical effects during braking. In previous work, a non-linear hardening model based upon the Chaboche plasticity model was isothermally [21,30] and anisothermally [22] calibrated using test specimens made from ER7 wheel steel. The primary differences between this implementation and the standard one is the addition of a thermal damage function to model pearlite spheroidisation and a radial hardness correction of the yield stress to mimic the actual hardness distribution that is present
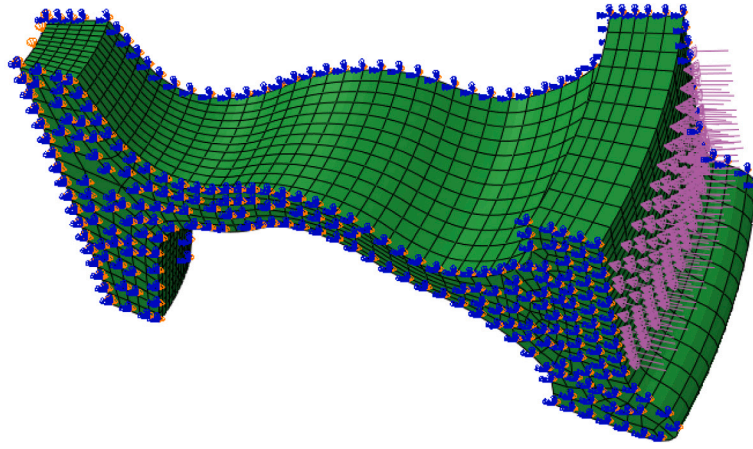
**Fig. 3.** Example of FE mesh of wheel sector used in analyses. Symmetry boundary conditions marked in blue and orange arrows (displacement/rotation), and heat flux surface indicated in purple. Sector angle is 20 degrees, corresponding to a hot spot wavelength of approximately 14.7 cm.
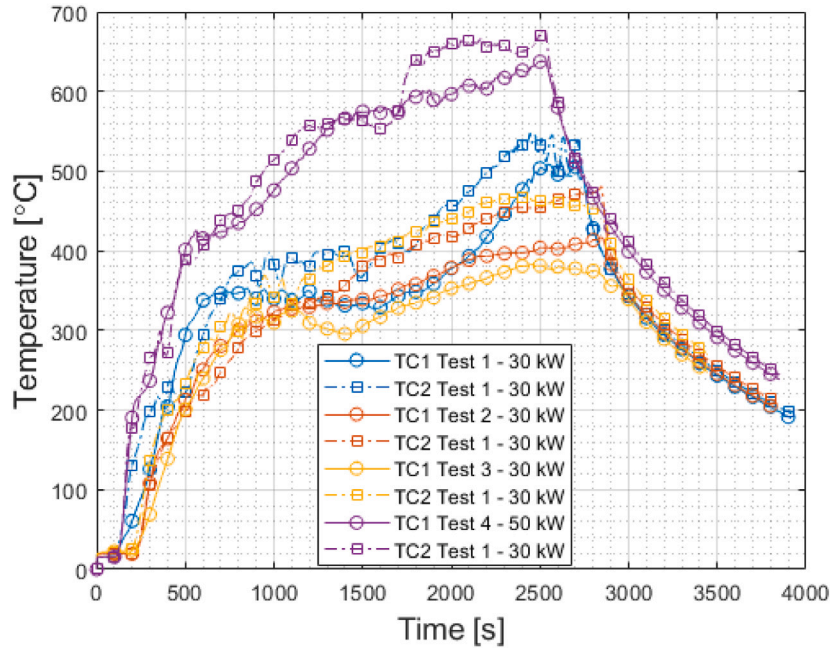


**Fig. 4.** Results from tests 1–3 for 30 kW braking and Test 4 for 50 kW. Note that the results from the sliding thermocouples are not related to the circumferential positions along the tread.

after manufacturing. The former approximates the material degradation/softening that occurs from the spheroidisation of the pearlitic by way of a differential

$$\dot{P} = \rho(P_\infty - P) \qquad (2)$$

where $P$ is the current hardness reduction, $P_\infty$ represents the final reduction and $\rho$ is a temperature dependent rate parameter. This is then applied to the yield stress and the plastic parameters. The model was implemented as a UMAT Fortran material subroutine in ABAQUS and is used in the mechanical analyses in the present work. The variation in hardness is accounted for by adjusting values of initial yield stress and plastic moduli by a relative factor normalised by 250 HV in the rim, which gives roughly a 20% decrease in the mentioned model parameters for the web and hub.

The mesh of a typical wheel sector employed in the parametric study is shown in Fig. 3. Only a 20° sector is used for the analyses as the highest tensile stresses are found in the hot spots themselves and the colder areas between hot spots, which show lower residual stresses,

are of no particular interest for this paper. The same mesh is used for both thermal and thermomechanical analyses. DC3D20 quadratic 20-node brick elements are used for the thermal analysis and C3D20 quadratic 20-node brick elements for the mechanical analysis. A mesh convergence study shows that the employed mesh gives good results for both thermal and mechanical simulations with deviations of single degrees or MPa. Furthermore, the volume-averaged stress evaluated later is not sensitive to peak values. The thermal boundary conditions are given by radiation defined directly within ABAQUS and convection via a Fortran FILM subroutine [6]. The thermal model was calibrated using experimental results from tests in a previous brake rig [7]. The convection and radiation coefficients vary depending on the location on the wheel, with e.g. metallic surfaces such as the wheel tread having lower emissivity. The radiation is modelled using the standard ABAQUS routines. The heat block is a good insulator and ≥90% [7] of the heat is assumed to enter the wheel. However, the aim is to mimic the temperatures seen in the experiments. This means that assumptions regarding the heat losses will not overly affect the results if the resulting
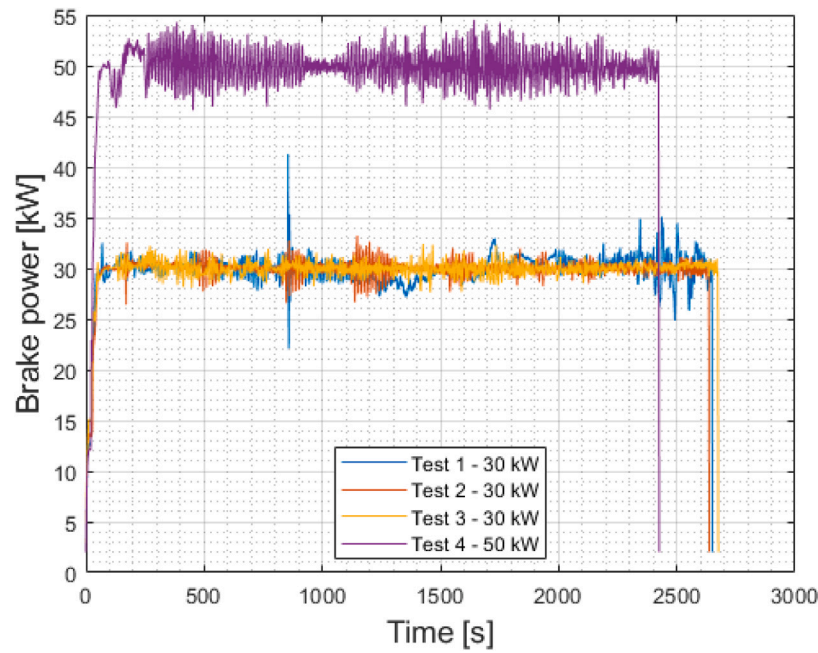
**Fig. 5.** Applied brake power during tests 1–3 for 30 kW braking and Test 4 for 50 kW.
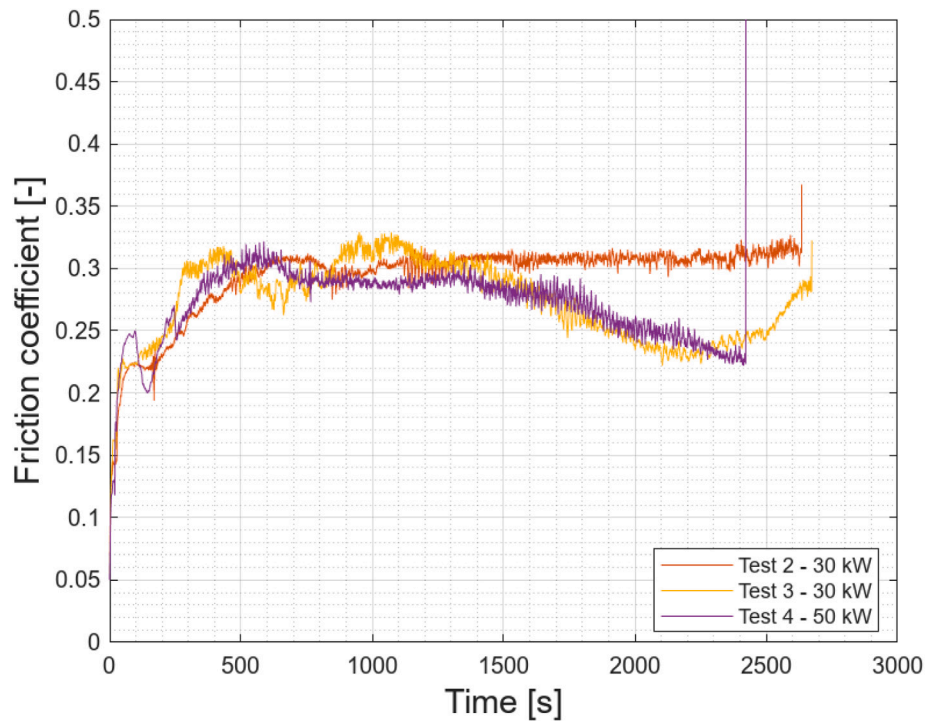


**Fig. 6.** Estimated friction coefficient during tests 1–3 for 30 kW braking and Test 4 for 50 kW. Note that the curve for Test 1 has been removed due to a faulty pnematuc pressure transducer.

temperatures are overall correct. The mechanical analysis has cylindrical symmetry boundary conditions on cross-sectional surfaces, and axial constraints on the hub bore (inner diameter) to prevent rigid body motion. The boundary conditions are indicated in Fig. 3. No mechanical load has been applied and the resulting stresses are only due to the thermal gradients. Since the wheel was used for some initial testing, the initial residual stress field that is induced from the manufacturing process has been somewhat modified. DUe to this, the distribution of residual stresses is also unknown and for simplicity it is assumed that the initial stresses in the wheel are zero. Comparison with other results

for wheels of the same type that have known testing histories show very similar stress results as those in this paper [31].

## 4. Results

The experimental results are presented in the first subsection, focusing on rim and tread temperatures and also on residual stresses, and, in the second subsection, finite element results detailing a parametric study on the influence of hot spots.
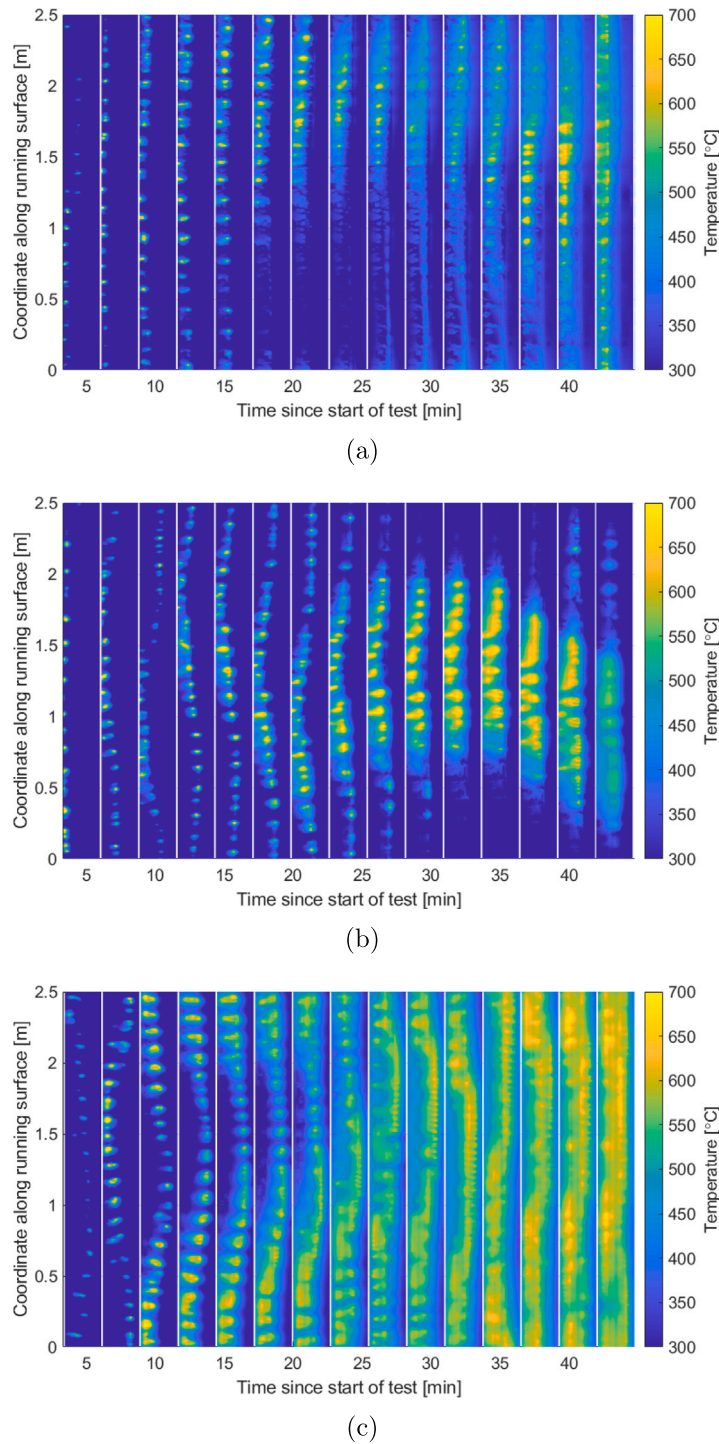
(a)



(b)



(c)

**Fig. 7.** Evolution of tread temperature at (a) first 30 kW braking, (b) second 30 kW braking, (c) 50 kW braking. One entire wheel revolution is given about every 3 min, with wheel flange side on the right.

### 4.1. Experimental results

Results from sliding thermocouples, as measured during the four test runs, are presented in Fig. 4. These results show that, even though the first three brake tests have identical brake power levels (30 kW), there are substantial differences in measured tread temperatures. This is so not only from test to test, but also when it comes to the two sliding thermocouples during one test. The average temperatures of the rim field side as captured by the thermographic camera can unfortunately

not be presented as they in parts were below the chosen calibration range of detectable temperatures. Brake power and estimated friction coefficients are shown in Figs. 5 and 6 respectively. The former indicates that the brake power is relatively stable on average, with some variation and short-lived spikes as the control system is not capable of handling the instantaneous changes that occur. The friction coefficient is overall stable for Tests 2–4 with values between 0.20 and 0.33. Not ethat no data are available from Test 1 due to a faulty pneumatic pressure transducer.
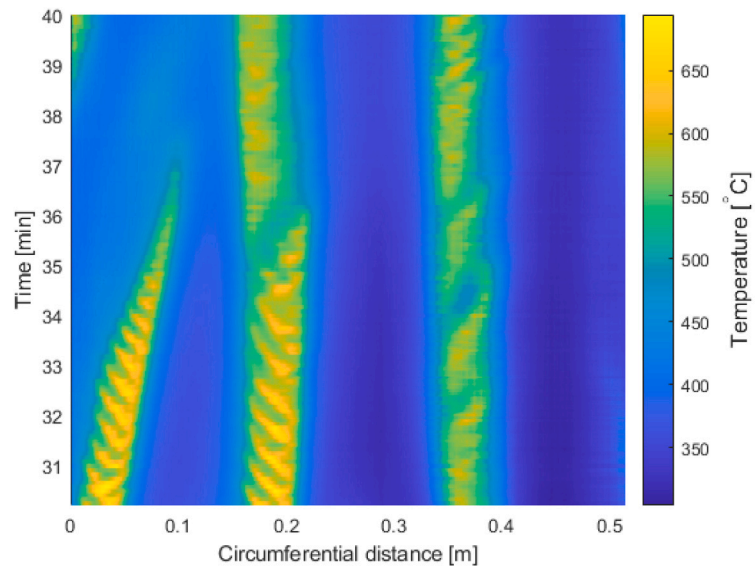
**Fig. 8.** Evolution of hot spot position on tread with respect to time as observed from mirror.
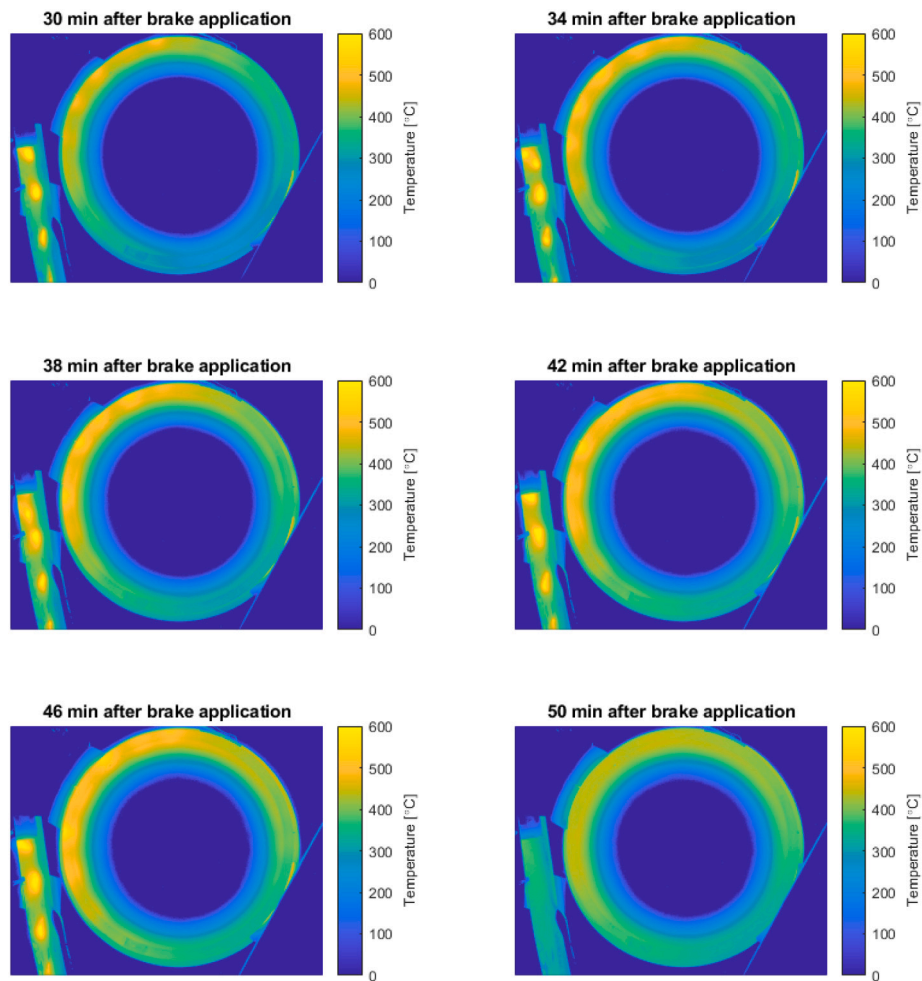


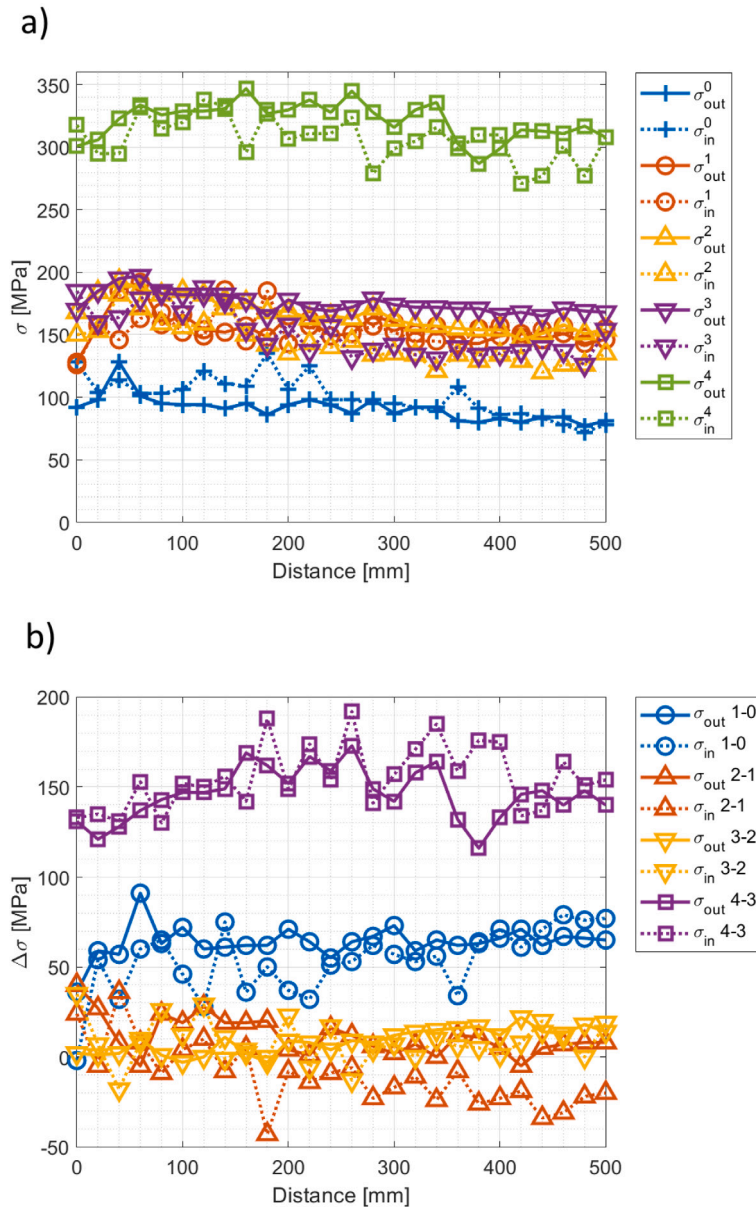**Fig. 9.** Wheel temperatures (°C) after indicated duration of braking for the third braking at 30 kW. Tread temperatures as seen in mirror to the left in the figures. Note different temperature scale compared to previous figures to improve visibility.

**Fig. 10.** (a) Measured residual stresses in wheel rim near to tread and web, marked "out" and "in", respectively. Data prior to testing are labelled "0" and after Tests 1 to 4 are labelled accordingly. Distance starting point is the unpainted area on rim field side. (b) Change in stresses resulting from test cycle. Markings "1-0" indicates change between tests labelled "0" to and test "1", and so on.

The wheel tread temperatures, for one entire revolution every 3 min, registered using the thermographic camera, are shown in Fig. 7. The images are limited to time intervals when the temperature was above 300 °C, since a high-temperature calibration range (300 °C to 1500 °C) was used for the majority of the tests. These tests indicate that hot spot temperatures are more than 200 °C higher than the background tread temperature. Furthermore, it is evident from the distributions that the locations of hot spots can be stationary, as seen in the first test at 30 kW in Fig. 7(a). Here the same hot spots as in the beginning appear at the end, indicating that they are stationary for some 30–40 min. Also the side view of the wheel for the third test at 30 kW in Fig. 9 shows that the distribution is nearly stationary. Furthermore, the hot spots observed in the mirror show only marginal migration during the braking event, see Fig. 8.

The hot spots can also be slowly migrating as in the second 30 kW test in Fig. 7(b). For the final experiment at 50 kW, see Fig. 7(c), the initial behaviour is similar to Fig. 7(a) with almost stationary hot spots, which then partially diffuse into hot sections over the tread during the

last 15 min of testing. The results also indicate that the hot sections are offset from the central tread, with elevated temperatures found towards the flange side.

Varying wavelengths of the hot spots of approximately 13–18 cm are seen in Figs. 7 to 9. From these results, it can be inferred that the hot spots are at least quasi-stationary, with any measurable movement occurring over several minutes. This is exemplified in Fig. 8, which showcases the movements of three hot spots during the test. Here, the two hot spots to the right in the figure keep their positions, whereas the one to the left migrates slowly to the right (towards the hot spot at the middle) and eventually fades away at time 38 min. Interestingly, soon after this, and at the very end of the test, a hot spot can be seen to reappear at about the same original position as the faded one (upper left corner of figure). This means that this position is again subjected to high temperature exposure.

The temperatures in Fig. 9 reveal that the wheel also has globally uneven temperatures, i.e. distributed with a single wave length around the wheel circumference. Measurements of out-of-roundness on similar
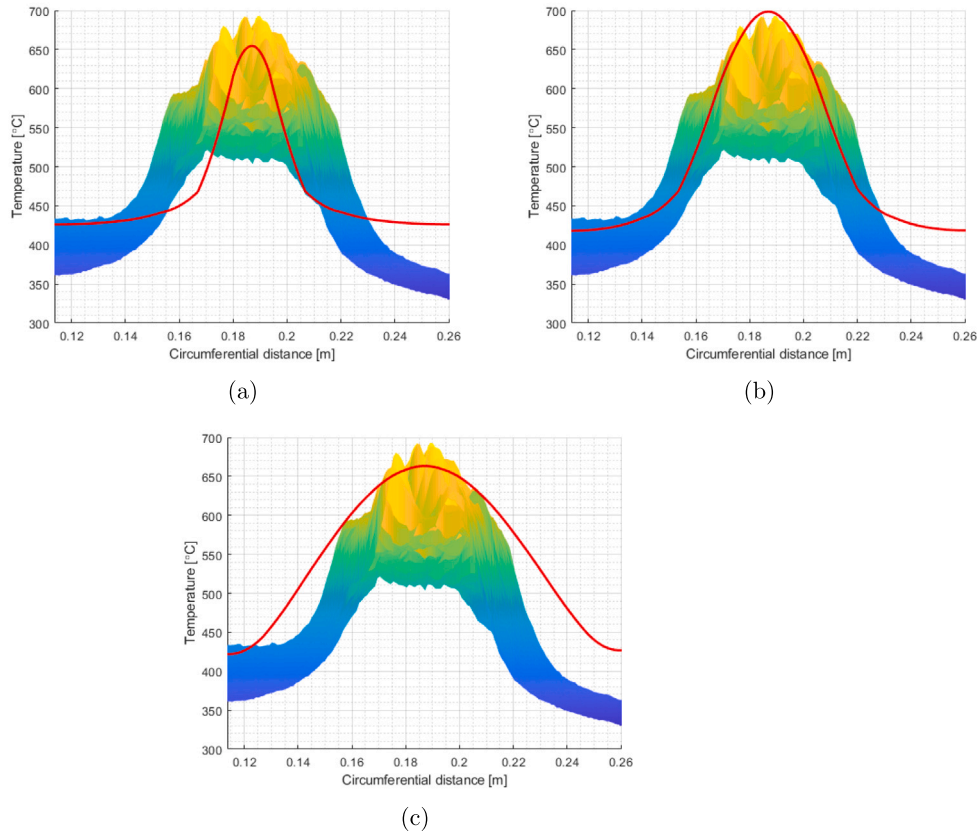
**Fig. 11.** Circumferential temperature distribution over the wheel segment corresponding to numerically studied hot spot sizes (a) 1.5 × 1, (b) 3 × 2 and (c) 6 × 4, compared to experimental measurements at end of 30 kW test. Calculated results (red lines) being compared to extracted tread temperatures over the circumferential length of one hot spot.
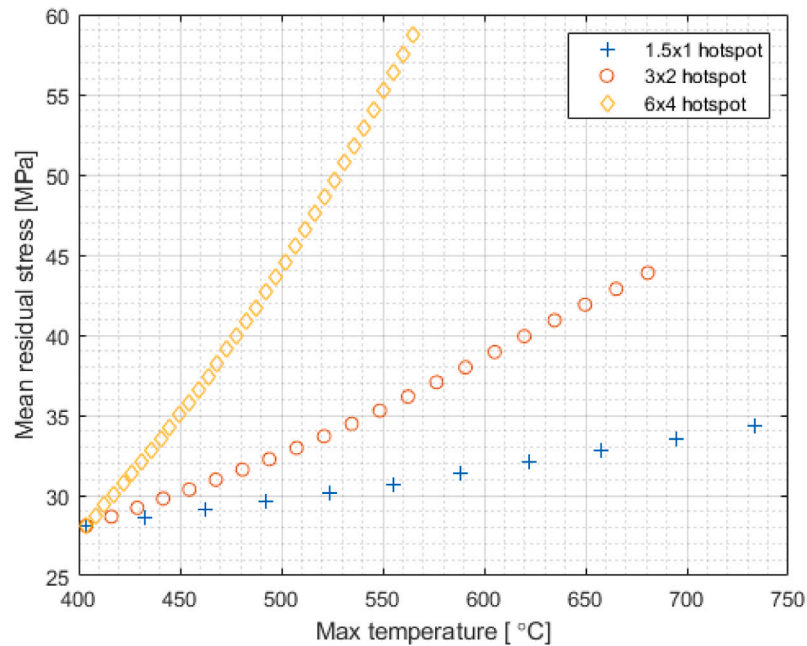


**Fig. 12.** Calculated mean residual stress of rim as functions of maximum temperature for three different hot spot sizes after braking at 30 kW during 45 min.

wheels suggest the evolution from an almost perfectly round wheel (0.06 mm deviation) prior to the first test, towards an out-of-round wheel after the final test (deviation of 0.17 mm). These measurements are performed on a cold wheel, and out-of-roundness on hot wheels may differ. This presents possible issues as the heat is concentrated towards one sector of the wheel. This has significant effects on the stresses and the thermally induced material changes in the wheel.

Residual stresses measured using the elastoacoustic effect, both prior to the tests and after each test, are presented in Fig. 10 over a 500 mm stretch of the rim starting from the unpainted mark on the
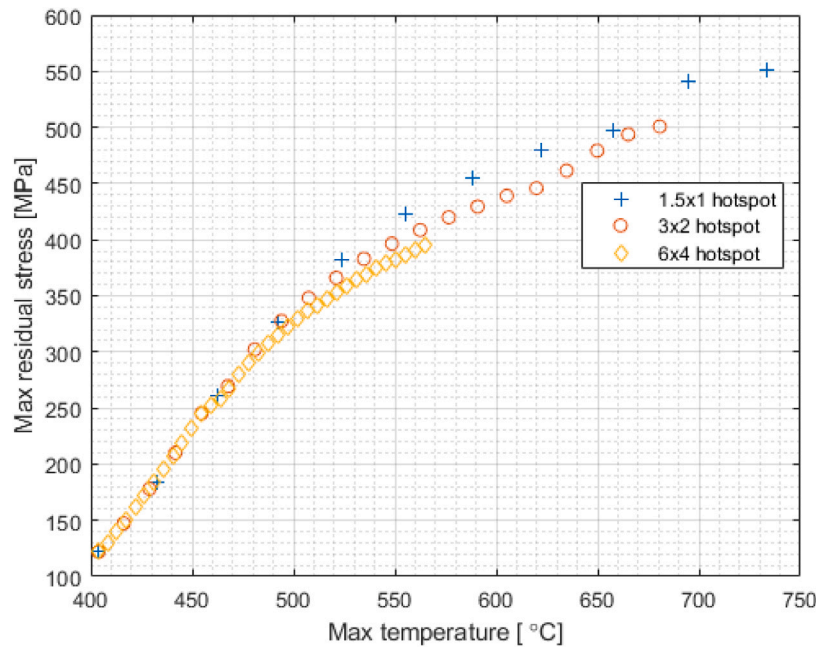
**Fig. 13.** Calculated maximum residual stress of rim as functions of maximum temperature for three different hot spot sizes for braking at 30 kW during 45 min.
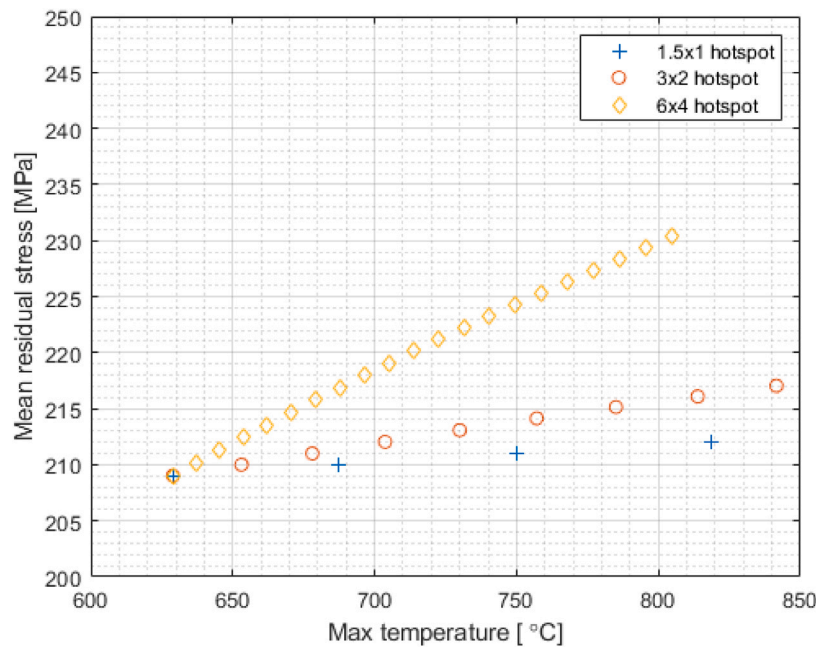


**Fig. 14.** Calculated mean residual stress of rim as functions of maximum temperature for three different hot spot sizes for braking at 50 kW during 45 min.

field side. At each position, one residual stress value is indicated for the outer and the inner part of the wheel rim, respectively, providing mean stresses over the entire width of the rim. Initial stresses in the rim are tensile and range between 75 MPa and 130 MPa. The first brake test at 30 kW increase the residual stresses near the tread by 40 MPa to 90 MPa along the studied 500 mm stretch of wheel rim. The two following 30 kW tests only marginally increase the residual stresses. The fourth test at 50 kW substantially increases the tensile residual stresses in the rim and they even exceed the permissible level 275 MPa [3]. After the 50 kW test there is also a substantial variation on stresses over the studied stretch of the rim, ranging between 270 and 340 MPa. The larger peaks and valleys are likely resulting from local thermal effects influencing the residual stresses.

### 4.2. Finite element results

First, simulated results are presented for a parametric study with maximum and mean residual circumferential stresses for three hot spot sizes. These are chosen with the semiaxes $a$ and $b$, as noted previously, being 1.5, 3 and 6 cm and 1, 2 and 4 cm, respectively. The maximum heat flux $q_{hs}$ added at a hot spot is chosen for each hot spot size to reveal interesting trends of temperatures and stresses. Included are studies on both 30 kW and 50 kW braking power. This is followed by a study on the effect the hot spots have on the distribution of the residual stresses in the rim.

The residual circumferential stress is evaluated by extracting the circumferential stress in the rim and then calculating mean and maximum values over the hot spot cross section, which coincides with
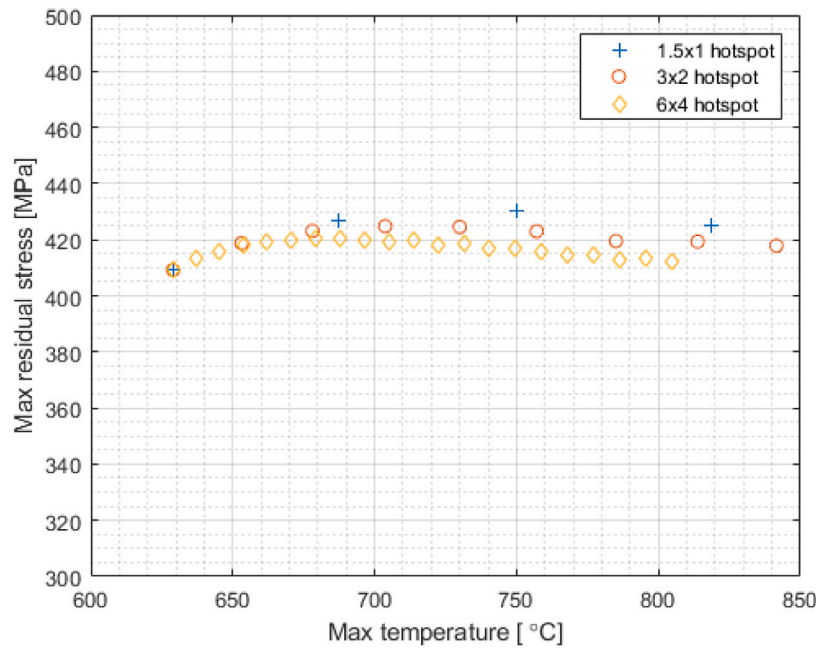
**Fig. 15.** Calculated maximum residual stress of rim as functions of maximum temperature for three different hot spot sizes for braking at 50 kW during 45 min.

the centre of the modelled sector. Other stresses are ignored as the values are significantly lower and the effective stress state is almost perfectly described by the circumferential stress. The mean stress value is found by averaging over the wheel rim cross-section, disregarding the flange. It should be noted that the values of the measured and simulated circumferential stress are not expected to match fully, since the braking history of the wheel is neither perfectly known nor accounted for in the simulation. Nevertheless, specific trends can be seen and compared.

Some calculated temperature distributions in the circumferential direction are shown in Fig. 11, where they are compared to data extracted from experimental results for the region close to one hot spot at the end of the 30 kW test. The designations correspond to the elliptical semiaxes $a$ and $b$ of the hot spots, where the first number is for $a$ (i.e. 1.5, 3 and 6 cm) and the second for $b$ (1, 2 and 4 cm), giving the different hot spots sizes as $1.5 \times 1$, $3 \times 2$ and $6 \times 4$. The ratio of 1:1.5 is to some extent based on the present experiments as well as values determined in [32]. A wide range of sizes/ratios are possible but given the qualitative analyses here this was determined to be sufficient. For this example, the simulated smallest hot with size $1.5 \times 1$ has a too narrow peak as compared to the chosen experimental result, the middle size $3 \times 2$ fits the data better, and the simulated largest size $6 \times 4$ has a too wide peak. During testing, examples of hot spots can also be found that are more narrow, closer to $1.5 \times 1$, and wider, closer to $6 \times 4$ cm. Additionally, issues arise due to the varying emissivity of the wheel tread and also from brake dust on the employed mirror that reduces the reflection. The former influences the temperature span and apparent sizes of hots spots, giving credibility to possibly an even larger variation in hot spot sizes, while the latter impacts the overall measured temperatures of the tread.

For the 30 kW simulations seen in Fig. 12, it is evident that both hot spots size and maximum temperature are important for mean residual stresses. The largest hot spot gives a substantial increase in mean residual stress. This is because the larger the hot spots is, more heat is applied at that hot spot area. For the largest, roughly 70% of the total power on the wheel sector is applied on the elliptic contact patch of the hot spot. This can be compared to maximum 40% and 20% for the smaller hot spots. As noted previously, the wheel design standard [3] states that the limit tensile residual stress for worn wheels is 275 MPa, implying that the here calculated stresses (lower than 60 MPa) are not

critical. However, hot spot sizes also have implications for the local stress field below the tread, which is discussed later.

The maximum residual stress on the tread on the other hand, shows a significant increase with the maximum hot spot temperature, regardless of hot spot size, see Fig. 13. It can be seen that tensile residual stresses of more than 550 MPa are induced when the maximum temperature reaches 750 °C. Such high residual stresses are not necessarily problematic as the high stresses are found only near the tread and not deeply penetrating into the rim. However, these stresses may still have implications for, e.g. initiation of surface cracks, which will be explored in future works.

Corresponding results are given for the 50 kW simulations in Figs. 14 and 15. Here, approximately 40% of the total heat flux is being applied to the large hot spot for the maximum temperature, and between 16 and 8% to the smaller ones. The chosen percentage values are empirically determined by comparing the highest temperatures between the simulations and the experiments. In Fig. 14 there is a slight increase in mean residual stress with higher maximum temperatures. The maximum stress is relatively constant for the entire surface which follows from the results in Fig. 15, with levels that actually are below those for the 30 kW case shown in Fig. 13. This is due to that prolonged exposure to high temperatures weakens the material, which means that the yield stress has been reduced in the employed material model.

The distributions of residual stresses throughout the rim for the various cases are shown in Fig. 16. For the 30 kW cases in Figs. 16(a), c and e, it is evident that despite the significantly higher temperatures of the $1.5 \times 1$ hot spot, the stress field only manages to penetrate to a relatively shallow depth, which has a low effect on calculated mean stresses. In comparison, the larger hot spots ($6 \times 4$) cause visible changes in the residual stress field to a significant depth, although the peak residual stresses at the centre of the hot spot are lower. For the 50 kW simulations, only small changes in the stress levels can be seen between the cases with no hot spot or a small hot spot, with all changes being concentrated towards the tread. In the simulation with the larger hot spot, however, deep penetration of elevated residual stresses is observed, with stress levels of approximately 400 MPa and above, halfways through the rim thickness.

On top of the temperature variations induced by the hot spots, the experimental testing also show global uneven heating around the wheel circumference. As can be noted in Figs. 7(a) and 7(b), the heating is not
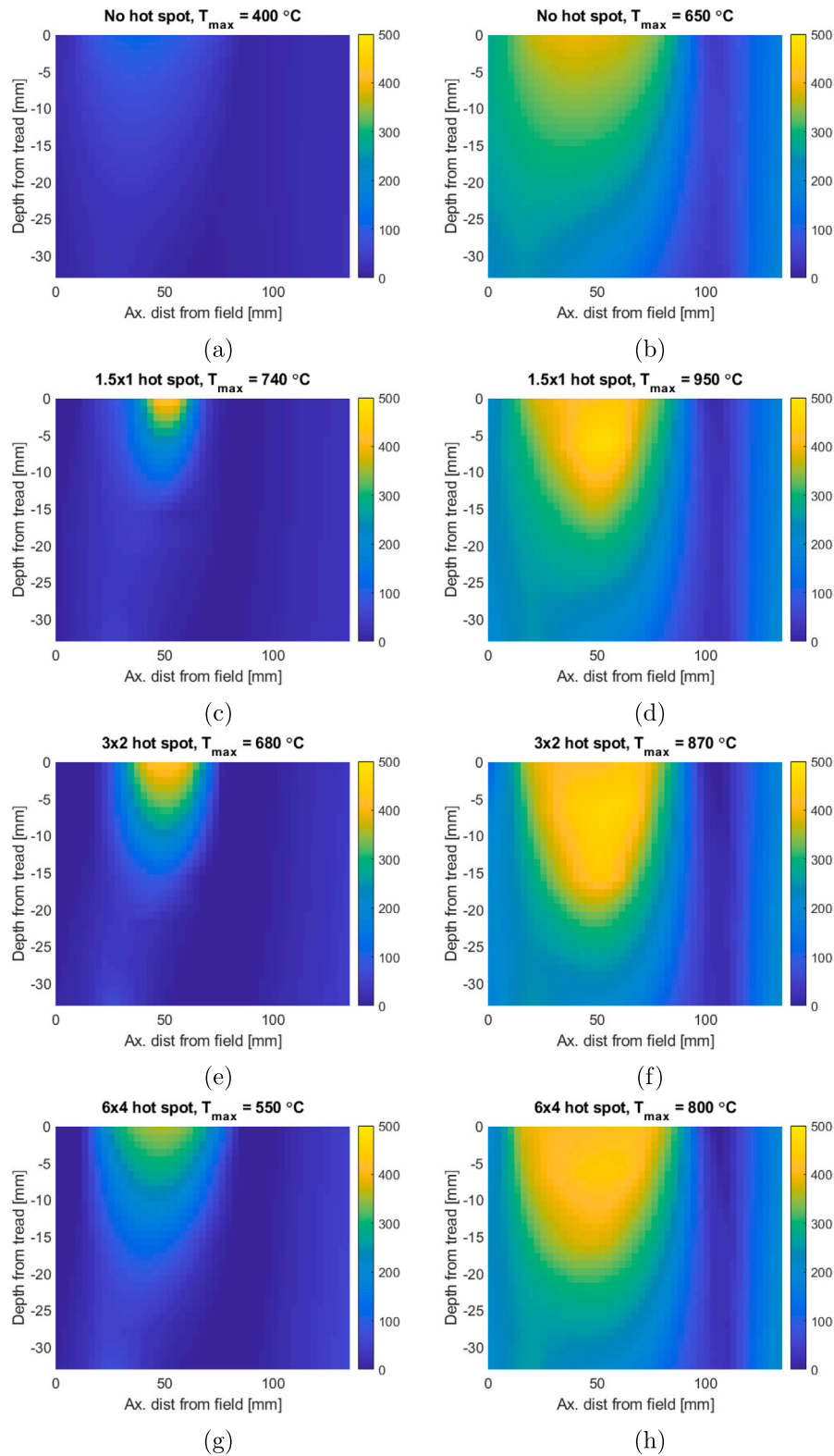
**Fig. 16.** Residual stress distribution in the rim for varying hot spots.
(a), (c), (e) and (g) are simulations for 30 kW braking and (b), (d), (f) and (h) are simulations for 50 kW. Hot spot sizes and maximum temperatures are indicated in figure titles.

distributed evenly over the circumference but has clustered to roughly a third to half of the wheel. This lends further credence that employing average temperatures as measured by, e.g. sliding thermocouples, may not be sufficient for characterising the wheel temperatures as the thermographic camera shows much higher peak temperatures. This

scenario has been numerically analysed in detail using a model of half of a wheel. The results are presented in Fig. 17, where temperatures from Fig. 7(b) are mimicked. It is found that a significant increase in tensile residual stresses results from such varying temperatures as compared to the case shown for uniform heating. The calculated mean
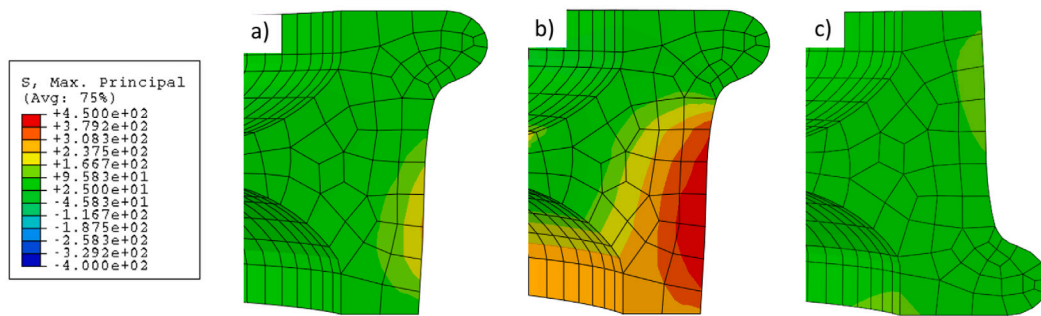
**Fig. 17.** Calculated residual stress distribution for wheels with (a) uniform heating and (b) subjected to global uneven heating as seen from thermographic camera in part of wheel with highest temperatures, and (c) in part of wheel with the lowest temperatures.

residual stress is for the section with highest temperatures 300 MPa, exceeding the allowed stress value 275 MPa stipulated in European standards. The section with the lowest temperatures meanwhile show stresses only slightly lower than the case with uniform heating.

### 4.3. Discussion

The overall findings from the numerical study, which build on experimental results, presents potential issues regarding stresses in wheels, with concentrated larger zones of elevated temperatures on the tread. The highest residual stresses in the wheel rim are concentrated towards the tread, which may increase the probability of crack initiation and possibly fracture in the wheel tread. This presents concerns as local stresses are difficult to measure non-destructively and that the mean stress, which can be measured, is only weakly affected by all but the largest simulated hot spot sizes. What is concerning is that, as seen in both Figs. 7 and 9, some form of localisation is occurring. Another aspect is that long-term exposure to high temperatures brings large-scale weakening of the wheel material, which also can influence crack initiation and growth but also tread wear characteristics. For the case with global uneven heating, temperature differences of more than 200 °C were observed on the wheel tread, meaning that material deterioration would start to occur in the hotter zones long before a thermocouple measurement of average temperature, or a numerical model that disregards such local heating effects, would indicate potentially detrimental temperature levels.

This also has relevance when comparing simulated and experimental results. The first measurement of the residual stress as seen in Fig. 10 shows values between 80 and 120 MPa, which lies somewhat above the results shown in Fig. 12. Slightly increased background heating or maximum temperatures closer to 600–650 °C for the 6 × 4 hot spot may cause this. This is also a reasonable approach, given that the temperatures as seen in Fig. 7(a) are slightly localised, suggesting that an approach with average temperatures of 500-550 °C on a larger zone than a 6 × 4 ellipse would be more suitable. For the second braking and onward, beginning with Fig. 7(b), the hot zone covers one-third to one-half of the wheel with temperatures up to 700 °C. With residual stresses of approximately 150–200 MPa for these experiments, it suggests that the assumption of 30 kW evenly distributed heat flux around the wheel circumference is not appropriate. Instead, the heat flux pertaining to the hot zone needs to be considered using a localised approach, where it is rather based on power levels 40 or 50 kW (with a corresponding decrease of heat flux outside of the hot zone). This is supported by the fact that the measured residual stress levels, averaged over inner and outer probe position, reach some 175 MPa, which approaches the simulated values in the 50 kW simulations.

is somewhat faulty. Instead, it may be that localised approaches using 40 or 50 kW are more accurate, in particular given that the measured residual stress levels of 200 MPa which approaches the simulated values in the 50 kW simulations.

### 5. Conclusion

A combined experimental-numerical study of the temperature distribution of a block braked railway wheel has been performed in order to investigate the effects of non-uniform temperature distribution induced at tread braking. Using a thermographic camera, it has been found that stationary hot spots often is a good assumption, although some variation is seen. In addition, the thermographic camera reveals globally uneven wheel temperatures around the wheel circumference which introduce substantial temperature variations during braking and wheel out-of-roundness upon cooling down. This will be further investigated in future papers. The finite element simulations generally predict increases of both mean and maximum residual stresses when hot spots are introduced. A significant increase in the mean residual stress at 30 kW is predicted with the inclusion of a large hot spot, however at an overall mean stress level that is low as compared to allowed levels stipulated in the European norm. For the 50 kW case the increase in mean stresses induced by hot spots is lower, but since the stresses here are more close to the allowed ones, the effect can be important for wheel integrity. A major impact on mean stresses is found for the case with global uneven heating of the wheel, with residual stresses superseding allowed levels. When it comes to local maximum stresses, they are highly affected by hot spots for the 30 kW case and the results reveal that the highest stress value on the tread basically is a function of the maximum tread temperature found at a hot spot, with only a small influence from hot spot size. Hot spots have a minor influence on the maximum stress level for the 50 kW case. The reason for this is that material weakening predicted from prolonged exposure to high temperatures occurs even without the addition of hot spots. Because of the weakening effect, the highest predicted stresses are actually lower than for the 30 kW case.

In conclusion, correct characterisation of heat flux on the wheel tread and the resulting temperatures is an essential aspect for ensuring good performance and safety during railway braking, especially in the case of larger hot spots or global uneven wheel heating. In future work, it would be worth investigating whether there are elevated risks of, e.g. wheel fracture or fatigue due to local stress effects and material weakening.

### CRediT authorship contribution statement

**Eric Voortman Landström:** Conceptualization, Data curation, Formal analysis, Investigation, Methodology, Resources, Software, Validation, Visualization, Writing – original draft, Writing – review & editing. **Tore Vernersson:** Conceptualization, Formal analysis, Funding acquisition, Investigation, Methodology, Project administration, Resources, Supervision, Validation, Writing – review & editing. **Roger Lundén:** Conceptualization, Funding acquisition, Project administration, Resources, Supervision, Writing – review & editing.

## Declaration of competing interest

The authors declare the following financial interests/personal relationships which may be considered as potential competing interests: Tore Vernersson reports equipment, drugs, or supplies was provided by Lucchini Sweden AB. Tore Vernersson reports equipment, drugs, or supplies was provided by Becorit GmBH. Tore Vernersson reports equipment, drugs, or supplies was provided by Faiveley Transport Nordic AB.

## Data availability

Data will be made available on request.

## Acknowledgements

## References

[1] Vernersson T, Lundén R. Temperatures at railway tread braking. Part 3: Wheel and block temperatures and the influence of rail chill. IMechE: J Rail Rapid Transit 2007;221(4):443–54.

[2] Teimourimanesh S, Lundén R, Vernersson T. Braking capacity of railway wheels – state-of-the-art survey. In: Proceedings of the 16th international wheelset congress. 2010, p. 18.

[3] EN 13979-1 Railway applications - Wheelsets and bogies - Monobloc Wheels - Technical approval procedure - Part 1: Forged and rolled wheels. Tech. rep. Brussels, Belgium: CEN; 2020.

[4] Parker R, Marshall P. The measurement of the temperature of sliding surface, with particular reference to railway brake blocks. Proc Inst Mech Eng 1948;158:209–29.

[5] Vernersson T. Tread braking of railway wheels - noise-related tread roughness and dimensioning wheel temperatures: field tests, rig measurements and numerical simulations, Doctoral Dissertation. Chalmers Appl Mech 2006;136.

[6] Vernersson T. Temperatures at railway tread braking. Part 1: Modelling. IMechE: J Rail Rapid Transit 2007;221(2):167–82.

[7] Vernersson T. Temperatures at railway tread braking. Part 2: Calibration and numerical examples. IMechE: J Rail Rapid Transit 2007;221(4):429–41.

[8] Dufrénoy P, Brunel J. Thermal localizations in friction brakes. In: Proceedings of the 26th Brake colloquium and exhibition. 2008, p. 9.

[9] Dufrénoy P, Weichert D. A thermomechanical model for the analysis of disc brake fracture mechanics. J Therm Stresses 2003;26:8:815–28. http://dx.doi.org/10.1080/01495730390207622.

[10] Teimourimanesh S, Vernersson T, Lundén R. Modelling of temperatures during railway tread braking: Influence of contact conditions and rail cooling effect. IMechE: J Rail Rapid Transit 2014;228(1):93–109. http://dx.doi.org/10.1177/0954409712465696.

[11] Teimourimanesh S, Vernersson T, Lundén R. Thermal capacity of tread-braked railway wheels. Part 2: Applications. IMechE: J Rail Rapid Transit 2016;230(3):798–812. http://dx.doi.org/10.1177/0954409714566057.

[12] Thuresson D. Thermomechanics of block brakes, Doctoral Dissertation. Chalmers Appl Mech 2006;156.

[13] Fec MC, Sehitoglu H. Thermal-mechanical damage in railroad wheels due to hot spotting. Wear 1985;102(1):31–42. http://dx.doi.org/10.1016/0043-1648(85)90089-4.

[14] Barber J, Beamond T, Waring J, Pritchard C. Implications of thermoelastic instability in automotive disc brakes under a drag brake application. ASME J Tribol 1985;107:206–10.

[15] Yeo T, Barber J. Finite element analysis of thermoelastic contact stability. ASME J Appl Mech 1994;107:919–22.

[16] Cookson J, Mutton P, Tran L, Qui C, Saporito R, Crew G. Tread damage due to extreme thermal localization under high braking loads in heavy haul operations. In: Proceedings 20th international wheelset congress. 2023, p. 5.

[17] Kato T, Kato H, Makino T. Effect of elevated temperature on shelling property of railway wheel steel. Wear 2016;366–367:359–67. http://dx.doi.org/10.1016/j.wear.2016.04.015.

[18] X8400sc user manual. Wilsonville, OR (USA): FLIR; 2013.

[19] DEBBIE user's manual. Warsaw, Poland: Debro UMS; 1996.

[20] Chaboche JL. Sur l'utilisation des variables d'état interne pour la description du comportementviscoplastique et de la rupture par endommagement. In: Proc. Problemes non-linéaires de mecanique, Symposium franco-polonais. 1979, p. 137–59.

[21] Chaboche JL. A review of some plasticity and viscoplasticity constitutive theories. Int J Plast 2008;24(10):1642–93. http://dx.doi.org/10.1016/j.ijplas.2008.03.009.

[22] Landström EV, Steyn E, Ahlström J, Vernersson T. Thermomechanical testing and modelling of railway wheel steel. Int J Fatigue 2023;168:107373. http://dx.doi.org/10.1016/j.ijfatigue.2022.107373.

[23] Datasheet Becorit 929-1. Recklinghausen, Germany: Becorit GmbH; 1999.

[24] EN 13979-1 Railway applications - Wheelsets and bogies - Monobloc Wheels - Technical approval procedure - Part 1: Forged and rolled wheels - FINAL DRAFT. Tech. rep. Brussels, Belgium: CEN; 2023.

[25] UIC Leaflet 541-4 5th Edition: Composite brake blocks - General conditions for certification and use, Union internationale des chemins de fer. Paris, France; 2018.

[26] NI cDAQ-9171/9174/9178 User Manual, https://www.ni.com/docs/en-US/bundle/cdaq-9171-9174-9178-features/resource/372838e.pdf.

[27] LABVIEW. Labview user manual. Austin, TX (USA): National Instruments; 2022.

[28] Sibin KP, John S, Barshilia C. Control of thermal emittance of stainless steel using sputtered tungsten thin films for solar thermal power applications. Solar Energy Mater Solar Cells 2015;133:1–7.

[29] ABAQUS. Abaqus analysis user's manual. Providence, RI (USA): Simulia, Dassault Systèmes; 2019.

[30] Esmaeili A, Ahlström J, Ekh M, Nikas D, Vernersson T. Modelling of temperature and strain rate dependent behaviour of pearlitic steel in block braked railway wheels. Railway Eng Sci 2021;29(4):362–78. http://dx.doi.org/10.1007/s40534-021-00244-z.

[31] Landström EV, Vernersson T, Lundén R. Proceedings 20th international wheelset congress. Improved finite element modelling of tread braked wheel performance verified by brake rig tests, 2023, p. 6.

[32] Esmaeili A, Singh Walia M, Handa K, Ikeuchi K, Ekh M, Vernersson T, et al. A methodology to predict thermomechanical cracking of railway wheel treads: From experiments to numerical predictions. Int J Fatigue 2017;105:71–85. http://dx.doi.org/10.1016/j.ijfatigue.2017.08.003.